

Trajectory Tracking Control of Dual-PAM Soft Actuator with Hysteresis Compensator

Junyi Shen¹, Tetsuro Miyazaki¹, Shingo Ohno², Maina Sogabe¹, and Kenji Kawashima^{1,*}

Abstract—Soft robotics is an emergent and swiftly evolving field. Pneumatic actuators are suitable for driving soft robots because of their superior performance. However, their control is not easy due to their hysteresis characteristics. In response to these challenges, we propose an adaptive control method to compensate hysteresis of a soft actuator. Employing a novel dual pneumatic artificial muscle (PAM) bending actuator, the innovative control strategy abates hysteresis effects by dynamically modulating gains within a traditional PID controller corresponding with the predicted motion of the reference motion trajectory. Through comparative experimental evaluation, we found that the new control method outperforms its conventional counterparts regarding tracking accuracy and response speed. Our work reveals a new direction for advancing control in soft actuators.

Index Terms—Soft Robotics, adaptive control, pneumatic actuators.

I. INTRODUCTION

Soft robotics, a field driven by flexible, lightweight structures with infinite degrees of freedom, offers a safe and natural human-machine interface during collisions or impacts [1]. This field has seen exceptional growth due to the development of soft actuators constructed from resilient materials, such as silicone rubber and shape memory alloys [2], [3]. These materials' innate flexibility provides soft robots the adaptability for diverse applications, ranging from medical devices and rehabilitation to industrial tasks [4]–[6].

Soft robotic motion depends on deformations of flexible actuators, with pneumatic actuation playing a significant role. Pneumatic artificial muscles (PAMs), based on the McKibben structure that replicates biological muscle movements, have been praised for their cost-effectiveness and high force-to-weight ratio [7]. Pneumatic bending actuators, typified by multiple miniature compartments, further advance this field, enabling more versatile movements and interactions [8]–[10].

While soft actuators' flexibility benefits soft robotics, it also introduces challenges, particularly in tasks requiring precision [11]. A significant hurdle is hysteresis — a nonlinearity makes the system complex to model and results in delayed actuator responses towards control signal changes, presenting challenges to rapid and accurate soft robotic control [12].

*This work has been submitted to the IEEE for possible publication. Copyright may be transferred without notice, after which this version may no longer be accessible.

¹Department of Information Physics and Computing, Graduate School of Information Science and Technology, The University of Tokyo, 7-3-1 Hongo, Bunkyo-Ku, Tokyo, Japan kenji.kawashima@ipc.i.u-tokyo.ac.jp

²Innovative Project Planning and Promotion Department, Bridgestone Corporation, 3-1-1 Kyobashi, Chuo-Ku, Tokyo, Japan shingo.oono@bridgestone.com

This issue is further augmented in pneumatic actuation due to the compressibility, limiting the application of pneumatic soft robots [8].

In addressing hysteresis, recent research has primarily embraced model-based control strategies and feedforward hysteresis compensation techniques [13]. The former conceptualizes hysteresis as an unmodeled dynamic or disturbance, aiming to attenuate its effects by complex nonlinear control algorithms [14]. Conversely, the latter leverages inversed hysteresis models derived through the amalgamation of assorted mathematical play operators [15]. However, model-based nonlinear algorithms hinge on accurate linear approximation, presenting a limitation. Meanwhile, feedforward hysteresis compensations demand substantial computational effort, both online for inversion processes and offline for hysteresis model construction, and encounter challenges in mimicking asymmetrical hysteretic traits [16]–[18]. The contemporary state-of-the-art primarily targets simple soft actuators possessing a singular degree of freedom (DoF) or multi-DoF actuators that can be segregated into elementary 1-DoF actuation units. Such prevalent methodologies may stumble when confronted with actuators exhibiting indivisible complex structures. Given the intrinsic complexities, potential unreliabilities of current methods, and their inadequacies for high-DoF actuators, the necessity for a straightforward yet efficacious anti-hysteresis control approach is accentuated [1], [10].

This work presents precise bending trajectory tracking control on a novel dual-PAM bending actuator. The architecture of this actuator features two antagonistically arranged PAMs. This arrangement melds the compact structure inherent in antagonistic mechanisms with the potentially adjustable stiffness and notable power-to-volume ratio provided by PAMs [19]. Unlike traditional parallel manipulators, whose motions can be dissected into simple linear motions of individual units [18], [20], our dual-PAM actuator facilitates bending actuation via the correlated continuum deformation of both PAMs alongside the elastic metal plate. This driving mechanism resists decomposition and straightforward modeling. In response to this challenge, we introduce a novel scheme termed *adaptforward* control. This strategy, rooted in the simple, effective, and ubiquitously employed PID controller, dynamically tunes the feedback gains based on the anticipated motion of the reference signal, thereby attenuating the hysteresis effects. Our proposed control method is substantiated through comparative motion tracking experiments.

The discourse unfolds as follows: Section 2 elucidates the dual-PAM soft actuator's design, mechanism, and hysteresis traits. Section 3 unveils the new control strategy. Section 4

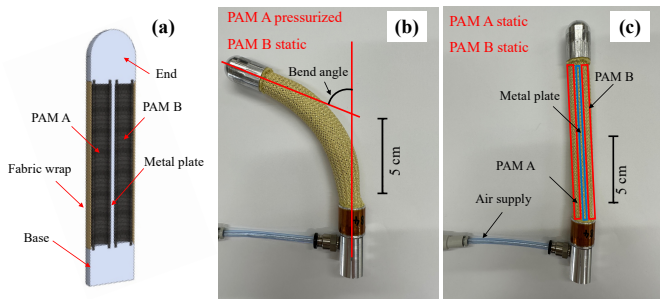


Fig. 1. Dual-PAM bending actuator: (a) longitudinal section, (b) single PAM being pressurized, (c) both PAMs at static state.

corroborates its effectiveness through experimental validation, juxtaposing its bending motion tracking accuracy against conventional methods. Section 5 encapsulates the conclusions.

II. DUAL-PAM SOFT BENDING ACTUATOR

A. Overall Configuration

Fig. 1 delineates the dual-PAM bending actuator employed in this study. The actuator's design encompasses a metallic base, a pair of rubber chambers, a metallic end, an elastic metal plate bridging the end and base, and a fabric sheath laterally enveloping the entire structure. This setup allows each chamber to operate as an independently controlled PAM; however, given their shared fabric sheath and common connection to the end and base, the actuation of each PAM is interdependent, resulting in an indivisible motion of the actuator and introducing specific modeling intricacies.

The actuator achieves controlled bending by the mechanism of PAMs. As illustrated in Fig. 1(b), when one single PAM is pressurized, it contracts and generates an axial tensile force toward the end. By creating an inflation differential between two PAMs, an imbalance in bending torques is established on either side of the metal plate, instigating its folding and propelling the actuator's motion. The antagonistic setup of the PAMs facilitates swift responsiveness to control signals and bidirectional bending capability, augmenting its adaptability in unknown environments as illustrated in Fig. 2. Moreover, this configuration permits potentially adjustable stiffness of the bending actuator through varying pressurization combinations.

The bending angle is modulated by altering the internal pressures within each PAM. In a fully depressurized state, the actuator swiftly reverts to its original straight configuration, as exhibited in Fig. 1(c). This recovery is ascribed to the elasticity of the metal plate, provided the applied torque remains within its elastic threshold, averting irreversible deformation and enabling natural reversion to the initial form.

Given the symmetrical bending performance inherent in the design of actuator, our motion tracking analysis is confined to unidirectional bending for reasonably minimizing the investigative workload.

B. Hysteresis Characteristics

1) *Experimental Apparatus*: We obtained bending-pressure hysteresis loops of the actuator by experiments. Experimental configuration is depicted in Fig. 3, encompassing components

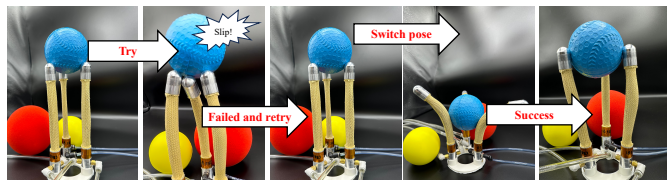


Fig. 2. Application of the dual-PAM actuator in soft grippers that can change poses for grasping objects with unknown structures.

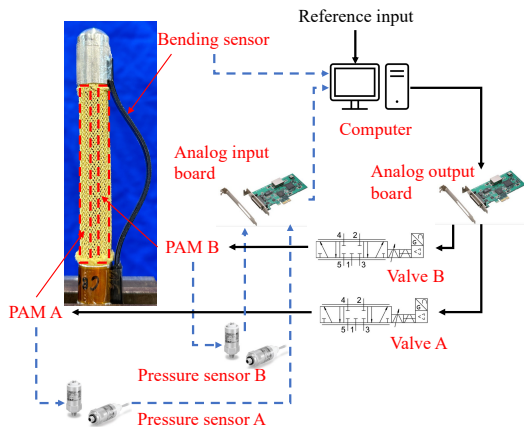


Fig. 3. Experimental apparatus.

include the dual-PAM actuator, a prototype provided by Bridgestone, a pair of Festo MPYE-5-M5-010B proportional valves, one BENDLABS-1AXIS angular sensor, two SMC PSE 540 A-R06 pressure sensors, and a computer system, within which a Contec AI-1616L-LPE and a Contec AO-1608L-LPE function respectively as the analog input board and the analog output board.

2) *Assessment of Hysteresis Loops*: Previous investigations into the hysteresis characteristics of PAMs employed triangular pressure waveforms originating from atmospheric states [15], thereby overlooking the hysteresis properties during transitions between depressurization and pressurization states at various deformation levels. To render a more comprehensive analysis of hysteresis properties, we design our assessment to encompass measurements of hysteresis loops emanating from two distinct initial states. In the first case, the internal pressures of both PAMs are set at atmospheric levels, with the initial bending angle defined as zero. Following this, a positive triangular waveform with diminishing amplitude alternately pressurizes and depressurizes PAM A, as demonstrated in Fig. 4 (a). The second scenario posits an initial pressure of 420 kPa within PAM A, with a subsequent application of a negative triangular waveform with diminishing amplitude to alternately depressurize and pressurize it, as depicted in Fig. 4 (b). The recorded minimum bending angle is designated as the zero-bending point in this latter measurement. Color distinctions within (a) and (b) delineate different input pressure cycles. Throughout the experimentation, continuous recordings of the actuator's bending angle and PAM A's internal pressure are maintained, while the internal pressure of PAM B is steadfastly held at the atmospheric value.

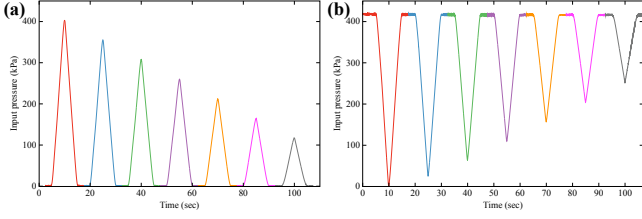


Fig. 4. Pressure variations in the active PAM: (a) pressurization from an atmospheric value, (2) depressurization from a pre-pressurized state.

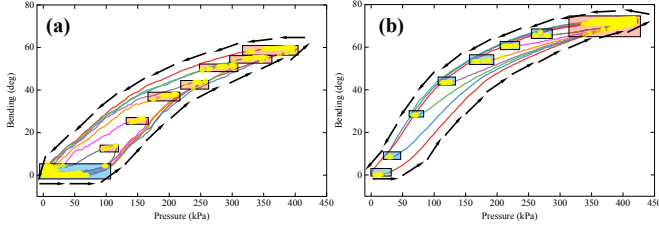


Fig. 5. Hysteresis loops: (a) results from Fig. 4 (a), (b): results from Fig. 4 (b). Golden shadows indicate points within hysteresis dead-zones.

The resultant hysteresis loops, corresponding to the distinct pressure variations, are illustrated in Fig. 5 (a) and (b), respectively. Arrows indicate the loop directions, with color variations aligning with the different pressure circles depicted in Fig. 4.

To analyze the hysteresis dead-zones and quasi-dead-zones within each loop, we delineate specific detection criteria. Initially, a positive-definite average angle-pressure gradient is computed from their respective variation range. The gradients between the angle and pressure of sample points located at 30 percent proximal to both ends of the pressure range are computed, with their absolute values compared with the calculated average gradient. Any gradient falling below 30 percent of the average gradient is identified as within the dead-zones or quasi-dead-zones. The process is succinctly delineated in Algorithm 1, where $gradientThreshold$ and $pressureThreshold$ are set to 0.3 and 0.2 respectively, conforming to our detection scheme. Pointed within dead-zone are accentuated by golden shadows in Fig. 5. Dead-zones manifesting during the state transition from pressurization to depressurization are denoted in red, while those during the depressurization to pressurization transition are masked in blue. An inspection of Fig. 5 (a) reveals an escalation in the widths of the red zones with increased bending angles. Conversely, Fig. 5 (b) exhibits an inverse correlation where the widths of the blue boxes amplify correspondingly with the diminution of bending angles. At highly pressurized states of the actuator, a noticeable increment in the width of blue boxes is captured with the escalation of bending angles, attributed to most part of the the hysteresis loop residing within the dead-zone as the actuator is highly deformed. The broadening of hysteresis deadzones signifies a magnification in the actuator's hysteretic properties, aligning with [21] that posits significant nonlinearities in PAMs when the actuator operates at extremely high or low pressurized levels.

Algorithm 1 Detection of Deadzone in Hysteresis Loops

Require:

$gradientThreshold$, $pressureThreshold$
 $hysteresisLoops$, $samples$

Ensure:

Identification of samples in deadzone

- 1: $gradThreshold \leftarrow gradientThreshold$
 - 2: $pressThreshold \leftarrow pressureThreshold$
 - 3: **for** each $loop$ in $hysteresisLoops$ **do**
 - 4: Compute average pressure: $P_{ave} \leftarrow (P_{max} + P_{min})/2$
 - 5: Compute positive-definite average gradient: $grad_{ave} \leftarrow (\theta_{max} - \theta_{min})/(P_{max} - P_{min})$
 - 6: **for** each $sample$ in $samples$ **do**
 - 7: **if** $|grad_{sample}| < gradThreshold \times grad_{ave}$
 - 8: **and** $|P - P_{ave}|/(P_{max} - P_{min}) > pressThreshold$ **then**
 - 9: Mark $sample$ as in dead-zone
 - 10: **else**
 - 11: Mark $sample$ as not in dead-zone
 - 12: **end if**
 - 13: **end for**
 - 14: **end for**
-

III. TRAJECTORY TRACKING CONTROL STRATEGY

Configuration of the dual-PAM actuator introduces a high-DoF nature into the control system, significantly complicating the application of model-based control algorithms or feed-forward hysteresis compensators. In this work, we deploy a feedback control system comprising two separated subsystems with cascaded loops and newly proposed adaptive hysteresis compensators. By adhering to only fundamental guidelines, our system design reduces efforts for alleviating hysteresis effects in precisely controlling soft actuators with complex structures.

A. Design of Control System

Our control system is designed in a discrete-time framework, utilizing k to signify the current time step and $k - i$ to represent the i th time step preceding the current. The architecture comprises two parallel subsystems, each embodying a cascaded structure with an outer loop dedicated to position control and an inner loop for pressure control. Both loops employ PID controllers, with each subsystem regulating a singular PAM of the actuator. This arrangement is depicted in Fig. 6, where black lines delineate forward paths from input reference value to output actual value, blue lines illustrate the feedback paths, and red lines display the adjustments delivered to the dynamic PID controller. An adaptive compensator is incorporated within each subsystem to account for hysteresis effects. Besides contributing to the adjustments in the pressure reference for the inner loop, the compensator also modulates the gain values of the outer loop PID controller. The pressure reference for the inner loops within both subsystems are computed as per

$$P_d(k) = P_d(k-1) + \Delta P_{fb}(k) + \Delta P_{ff}(k). \quad (1)$$

Given the symmetry of the system structure, designations *A* and *B* to specify different subsystems are omitted herein for brevity.

B. Design of Adaptive Hysteresis Compensator

Fig. 7 illustrates the proposed adaptive hysteresis compensator, encompassing an adaptive program alongside a feedforward differential (D) controller. In this configuration, $\tilde{\theta}_d^{(i)}$, ($i \geq 1$) denotes the i -th order pseudo-differential of the reference bending angle. The feedforward D gain, K_{ff} , operates as per

$$\Delta P_{ff}(k) = K_{ff} \tilde{\theta}_d^{(1)}(k), \quad (2)$$

and aims to mitigate the intrinsic response delay within feedback control and the deformable soft actuator [23]. The computed ΔP_{ff} is thereafter merged with the pressure adjustment ΔP_{fb} emanating from the outer loop PID controller, jointly serving as an adjustment to the inner loop's reference.

Incorporating the feedforward factor proves notably advantageous when the desired bending undergoes significant variation, exhibiting a correspondingly high differential value. Contrarily, the adaptive program is expected to operate when the reference changes slightly, where the feedforward component exerts limited effort due to low differential values. The adaptive program processes the reference signal along with its first and second pseudo-differential values, subsequently delivering adjustments to the PID controller nested within the outer position loop, thereby dynamically altering its proportional gain.

To facilitate a streamlined tuning process of PID gains, a regimen was devised where the variations in internal pressure adjustments within the antagonistic PAMs are engineered to reflect each other inversely. Consequently, PID gains in the outer loops of both subsystems and the feedforward differential gains are assigned opposite signs. Concurrently, parameter configurations of the adaptive program—elaborated in the ensuing subsection—are harmonized across different subsystems. Additionally, identical PID gains are allocated for inner loops across different subsystems to ascertain consistent performance in pressure control.

C. Adaptive Law of Dynamic Proportional Gain

Prior to expounding on the adaptive rule depicted in Fig. 7, it is imperative to elucidate several pivotal facets pertinent to bend motion tracking control employing pneumatic soft actuators. (1) Hysteresis-induced delay in actuator response primarily surfaces during state transitions between pressurization and depressurization, typically aligning with turnings in the target motion where the velocity direction alters. (2) Given any existing target's continuous movement, a deceleration-hold-acceleration sequence is inherent to any directional change in the tracked motion. (3) In the absence of rapid shifts in the tracked motion, the reference can be deemed in a quasi-static state, wherein augmenting the proportional gain of conventional PID controllers can enhance tracking performance [24]. However, an excessive gain increase might instigate instability during large-scale reference changes, as dynamic motion tracking typically demands more stringent

gain margin requirements [25]. (4) Given the frequency invariance of the hysteresis property [26], a viable mitigation strategy involves altering the control signal drastically, thus compelling the system to pass hysteresis dead-zones quickly.

Aiming for design generality, our adaptive program is architected to process the reference signal in real-time. The program employs velocity and acceleration data from the reference motion to foresee its variation and accordingly modulate the dynamic proportional gain. Given the nonlinear control system's complexity, deriving a precise one-to-one relationship between the dynamic PID gain and the reference signal is scarcely feasible. Moreover, an exact linear relationship could lead to significant dynamic gain fluctuations due to oscillations in real-time discrete pseudo-differential values resulting from unequal sampling intervals, which may subsequently induce system instability. Hence, we propose the adaptive law premised on an accumulative operation. Initially, given a negative acceleration of the reference angle $\tilde{\theta}_d^{(2)}(k)$, the dynamic proportional gain adjustment $\Delta K_P(k)$ is expressed as:

$$\Delta K_P(k) = M_1 \frac{\theta_d(k)}{a_1} \frac{b_1}{b_1 + |\tilde{\theta}_d^{(1)}(k)|} \frac{|\tilde{\theta}_d^{(2)}(k)|}{c_1 + |\tilde{\theta}_d^{(2)}(k)|} D(k). \quad (3)$$

Contrarily, for positive $\tilde{\theta}_d^{(2)}(k)$ values, the adjustment $\Delta K_P(k)$ is determined by

$$\Delta K_P(k) = M_2 \frac{\Theta - \theta_d(k)}{a_2} \frac{b_2}{b_2 + |\tilde{\theta}_d^{(1)}(k)|} \frac{|\tilde{\theta}_d^{(2)}(k)|}{c_2 + |\tilde{\theta}_d^{(2)}(k)|} D(k). \quad (4)$$

In other circumstances, $\Delta K_P(k)$ defaults to 0.

In the aforementioned definitions, $\theta_d(k)$ denotes the reference bending angle, Θ signifies its predetermined variation range, and $K_P(0)$ represents the initial proportional gain of the PID controller. The term a models the correlation between the width of hysteresis dead-zones and current deformation level, as observed in Fig. 5. Term b ensures a smooth variation in the proportional gain, limiting gain augmentation during drastic tracked motion changes while facilitating rapid gain increase as the reference change decelerates. Term c , the acceleration coefficient, ensures adjustable amplification in dynamic gain with the angular acceleration of the reference bending. By tuning a , b , and c values, the system can exhibit adjustable anti-hysteresis performance, with the asymmetry in hysteresis loops being addressable by assigning different values to parameters with differing footnotes (i.e., 1 or 2 in Eq. (3), and Eq. (4)). $D(k)$ is a direction changer defined by

$$D(k) = - \left(1 + \frac{1 + h(k)}{2} \cdot \mu \right) h(k), \quad (5)$$

where $h(k)$ is a sign function $h(k) = \text{sgn}(\tilde{\theta}_d^{(1)}(k) \tilde{\theta}_d^{(2)}(k))$, and μ is an augment operator used to impose a natural decreasing tendency to the dynamic proportional gain for maintaining system stability from sustained high gain values. To uphold a baseline of the dynamic proportional gain as $K_P(0)$, a cutoff operation

$$K_P(k) = \max\{K_P(0), K_P(k-1) + \Delta K_P(k)\} \quad (6)$$

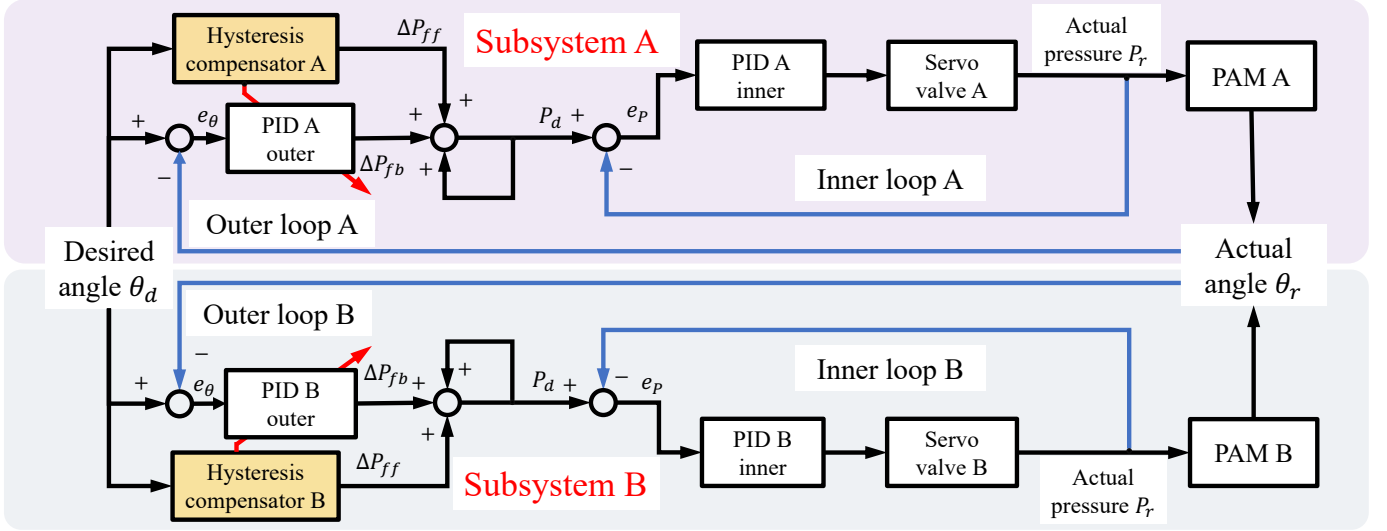


Fig. 6. Schematic of the control system with two subsystems independently governing two PAMs.

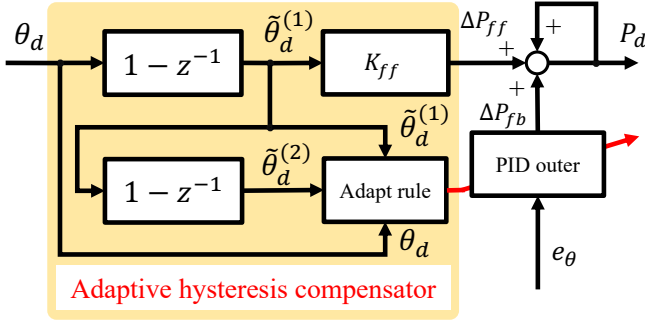


Fig. 7. Architecture of the adaptive hysteresis compensator.

is performed with each update. Lastly, M ensures formal dimensional consistency on both sides. By redefining parameters as $M^* = M \cdot b/a$, Eq. (3) can be rephrased as

$$\Delta K_P(k) = M_1^* \frac{\theta_d(k) |\tilde{\theta}_d^{(2)}(k)|}{(b_1 + |\tilde{\theta}_d^{(1)}(k)|)(c_1 + |\tilde{\theta}_d^{(2)}(k)|)} D(k), \quad (7)$$

and Eq. (4) can be expressed by

$$\Delta K_P(k) = M_2^* \frac{(\Theta - \theta_d(k)) |\tilde{\theta}_d^{(2)}(k)|}{(b_2 + |\tilde{\theta}_d^{(1)}(k)|)(c_2 + |\tilde{\theta}_d^{(2)}(k)|)} D(k). \quad (8)$$

IV. EXPERIMENTAL VALIDATION

A. Experimental Setup

Efficacy of the proposed method is ascertained through a series of experiments, with the performance disparities between the novel approach and the conventional PID control being delineated through the tracking of three different references. Comparative analyses among traditional PID (PID), PID augmented with a feedforward differential element in the hysteresis compensator (PID+FF), and PID with the entire function of hysteresis compensator (PID+AF) are conducted by tracking sinusoidal references of varying amplitudes and frequencies. The comparative results are tabulated for clarity.

The centroid of the diverse sinusoidal references is fixed at 30° . In the frequency evaluation, the amplitude is maintained at 20° , rendering a reference bending range from 10° to 50° , with periods of 10s, 8s, 6s, 4s, and 2s. In the amplitude analysis, the period is fixed at 8s, while amplitudes of 10° , 15° , 25° , and 30° are tested, given that a 20° amplitude is employed in the frequency test. Owing to the challenges posed in employing either the model-based nonlinear control algorithms or play-operator-based hysteresis compensation techniques for controlling this multi-DoF actuator, comparisons with these methods are omitted in this work.

Given that the dynamic gain value in the proposed scheme is contingent on historical reference signals in a short horizon, the demonstrative experiment is designed wherein the reference signal is cyclically applied thrice, with the central application taken as the experimental result to obviate the performance variance induced by initial conditions. Analogously, each sinusoidal reference signal in our amplitude and frequency test is applied across seven periods, with results from the central five periods selected for similar reasons.

Each experiment is repeated five times, and obtained data are processed independently with the mean values depicted in figures and tables. Considering environmental uncertainties, we use solid lines to represent the average result across different trials, and use shaded regions to denote the variations between the maximum and minimum values. A sampling frequency of 500 Hz is employed for capturing reference signals, actual bending angles, PAM pressures, and updating the proportional gain during the experiments. Via trial and error, parameters within the control system were ascertained: the gains for PID controllers in cascade loops, the feedforward D gain in the hysteresis compensator, and all coefficients utilized in the adaptive program. Identified settings are tabulated in Table I and II. To economize on space, only the PID gains in subsystem A are tabulated, with the gain values for subsystem B being inferable from the system design exposition in the preceding section.

TABLE I
PID GAINS IN SUBSYSTEM A.

Parameter	Value	Unit
Inner - P	4.0×10^{-2}	V/kPa
Inner - I	2.0×10^{-6}	V/kPa · s
Inner - D	0	V · s/kPa
Outer - P	8.0×10^{-2}	kPa/deg
Outer - I	2.0×10^{-5}	kPa/deg · s
Outer - D	0	kPa · s/deg
Feedforward - D	1.0×10^{-2}	kPa · s/deg

TABLE II
PARAMETERS IN ADAPTIVE RULE.

Parameter	Value	Unit
M_1^*	6.0×10^{-2}	kPa/deg · s
b_1	6.0	deg/s
c_1	3.2×10^4	deg/s ²
M_2^*	9.6×10^{-2}	kPa/deg · s
b_2	6.0	deg/s
c_2	5.0×10^4	deg/s ²
Θ	60	deg
μ	0.6	/

B. Experimental Results and Discussion

Experimental outcomes of tracking three demonstrative references are depicted in Fig. 8, 9, and 10. It's observed that performance of the traditional PID control greatly deteriorates with the increasing amplitude and frequency of the reference signal, especially when it turns. Conversely, the proposed PID+AF method bolsters the system's dynamic tracking accuracy, ensuring close adherence to the target across various amplitudes and frequencies. The delay in response, attributable to hysteresis, is perceptible in the error patterns; where the errors under PID control exhibit regular fluctuations with changes in the reference signal while these fluctuations are markedly subdued in the PID+AF control.

The effects of unequal sampling intervals on discrete pseudo-differential operations results in fluctuations in the

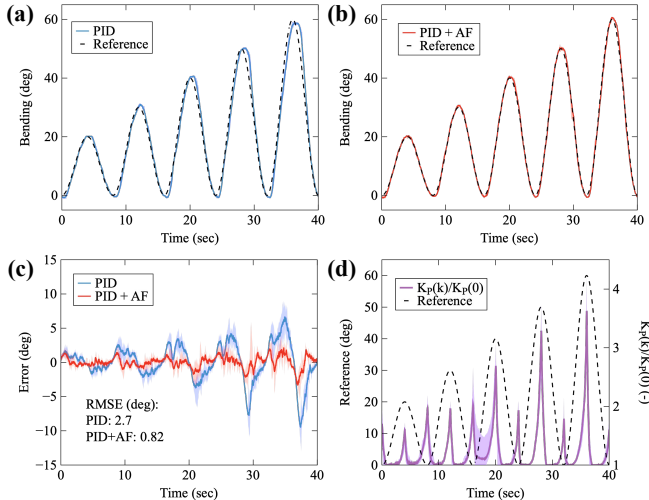


Fig. 8. Tracking result 1: (a) PID, (b) Proposed *adaptforward*, (c) Tracking errors, and (d) Dynamic gain amplification.

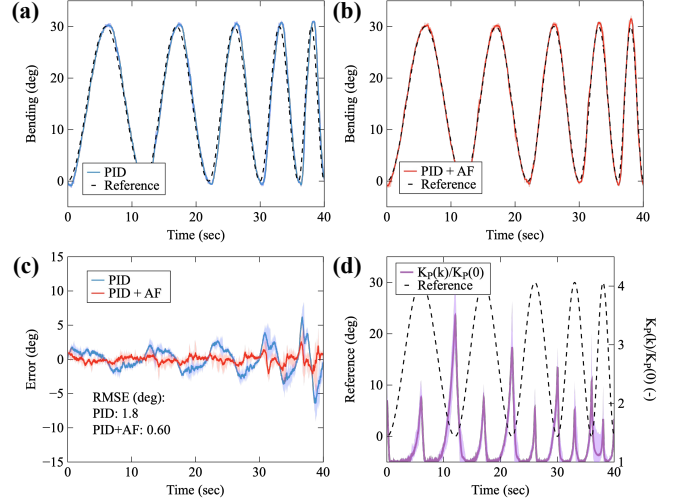


Fig. 9. Tracking result 2: (a) PID, (b) Proposed *adaptforward*, (c) Tracking errors, and (d) Dynamic gain amplification.

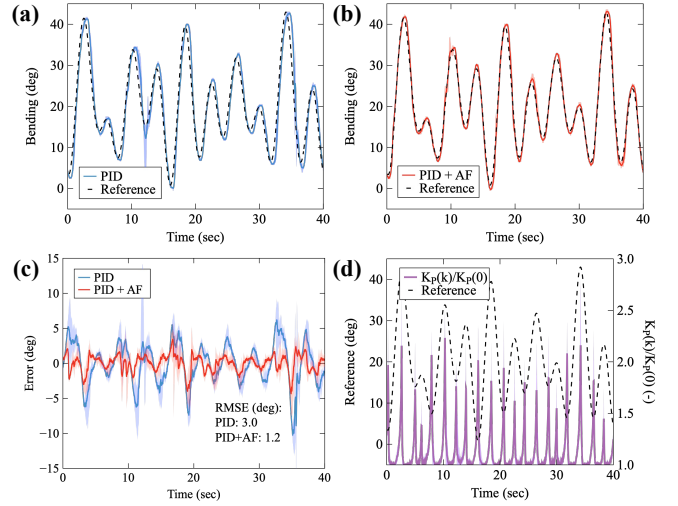


Fig. 10. Tracking result 3: (a) PID, (b) Proposed *adaptforward*, (c) Tracking errors, and (d) Dynamic gain amplification.

dynamic gain value, as evidenced by the wide shadow ranges in Fig. 8 and 9. However, the adaptive gain demonstrates a steady decline to a low value as the reference exits its turning region, thanks to the imposed natural decreasing tendency. In the case of the compound signal with irregular and frequent changes, fluctuations in response are discernible in both PID and PID+AF results, as showcased in Fig. 10. Nevertheless, the system maintains stability throughout the repeated experiments. A comparative assessment of the shadow zones reveals that the PID control, despite employing a more conservative constant gain, exhibits more pronounced fluctuations and overshoots due to significant tracking errors in feedback adjustment, as opposed to the more stable performance exhibited by the proposed method.

The performance evaluation of diverse control methodologies across varying reference signals is encapsulated in Table III and IV. A notable degradation in accuracy is observed with

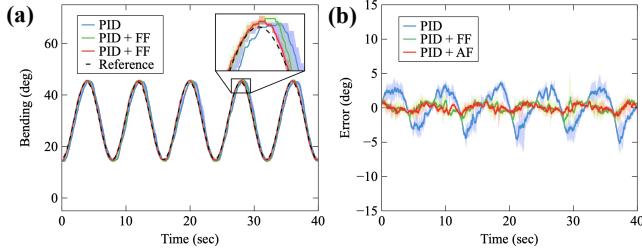


Fig. 11. Tracking results of the reference with an amplitude of 15° .

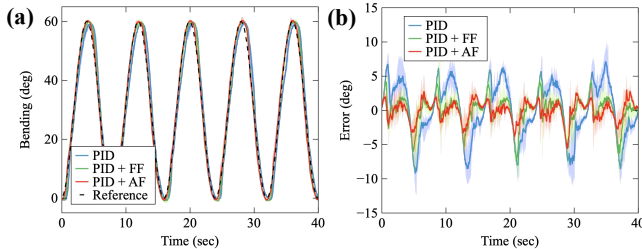


Fig. 12. Tracking results of the reference with an amplitude of 30° .

escalating frequency and amplitude of the reference for all control approaches. The conventional PID controller exhibits the poorest performance across all experimental scenarios. Incorporating the feedforward differential element (PID+FF) enhances the performance of PID, and a further enhancement is realized through deploying the proposed adaptive scheme (PID+AF). Compared to the performance disparity between the conventional PID control and our proposed method, the PID+AF delineates a less pronounced enhancement relative to the PID+FF. This occurrence is attributed to the pivotal role the feedforward differential component plays in elevating the efficacy of the PID control mechanism. On the other hand, the adaptive facet is conceived as a compensatory adjunct to the feedforward differential, particularly at the inflection junctures, where differential values of the reference descend.

Fig. 11 and 12 delineate the tracking performance for signals with a low amplitude (15° to 45°) and a high amplitude (0° to 60°), respectively. For lower amplitudes, PID control alone manifests notable response delays. As amplitude intensifies, discrepancies between actual and reference signals at trajectory turning points become apparent. Both PID+FF and PID+AF methods ameliorate this discrepancy, attributing to the rapid response brought by the feedforward element. PID+AF exhibits minimal shifts among different methods, indicating its superior responsiveness to reference alterations. The efficacy of PID+FF dwindles at trajectory turning zones due to the correspondingly low differential values, resulting in suboptimal tracking at these junctures. Conversely, the augmented feedback gains of PID+AF at such regions counteract this performance degradation, engendering enhanced tracking performance.

Figures 13 and 14 depict the results for tracking reference signals with a long period (6s) and a short period (4s), respectively. Analogous to amplitude analysis, PID control manifests a notable lag at lower frequencies. The PID+AF

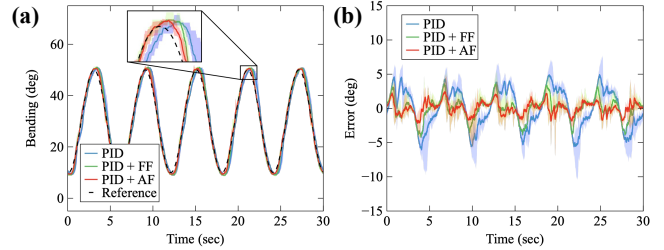


Fig. 13. Tracking results of the reference with a period of 6s.

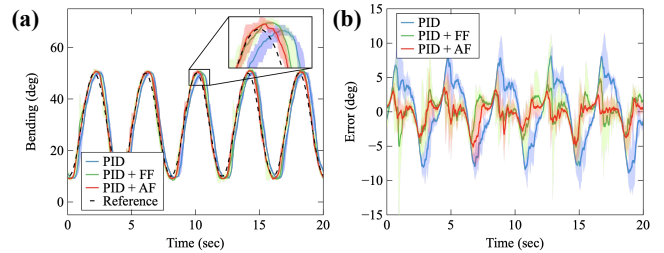


Fig. 14. Tracking results of the reference with a period of 4s.

method's improvement becomes less prominent as frequency elevates, as depicted in Fig. 14, owing to the predominant error source transitioning from hysteresis to the incompatibility between PID settings and high-frequency signals, which is evidenced by the substantial fluctuation ranges in PID's response. Although its superior performance is underscored in Table IV, the proposed PID+AF fails to fully counteract this incompatibility between feedback settings and reference signal characteristics.

V. CONCLUSION

We achieved precise bending trajectory tracking control on a dual-PAM bending actuator paired with an adaptive control scheme. The bending actuator comprises two independently controlled PAMs, separated by a central metal plate, with its bending motion hinging on the continuum deformation of both PAMs and the metal plate. Through experimentation, the hysteresis characteristics of this pneumatic actuator were scrutinized, revealing the interrelation between the hysteresis dead-zone widths and the level of deformation.

A control system was introduced for precise bending control by amalgamating two cascaded PID loops with newly proposed adaptive hysteresis compensators. The compensator contains an adaptive program and a feedforward differential controller. Leveraging the predicted motion of reference signals, the adaptive program facilitates dynamic adjustments in the proportional gain of the PID controller for precise bending manipulation. The proposed control method, aimed at curtailing hysteresis-induced tracking errors, was experimentally validated on a series of reference signals.

Our engineered strategy is simplistic yet potent in controlling actuators manifesting hysteresis, thereby expanding the vista for soft actuator applications in robotics and automation.

TABLE III

PERFORMANCE METRICS FOR TRACKING REFERENCES OF DIFFERENT AMPLITUDES, WITH RESULTS FORMATTED AS PID+AF (PID, PID+FF).

Amplitude [deg]	MAE [deg]	RMSE [deg]	e_{\max} [deg]	e_{\min} [deg]	Var [deg ²]
10	0.42 (1.3, 0.56)	0.51 (1.5, 0.83)	1.6 (3.3, 2.6)	-1.7 (-4.0, -2.8)	0.26 (2.3, 0.73)
15	0.53 (1.9, 0.78)	0.66 (2.3, 0.94)	2.0 (4.5, 2.8)	-2.3 (-5.9, -2.9)	0.44 (5.3, 0.88)
25	0.88 (2.5, 1.4)	1.2 (3.1, 1.7)	3.8 (6.6, 4.1)	-4.3 (-8.3, -5.7)	1.5 (9.4, 2.9)
30	1.2 (3.4, 1.8)	1.7 (4.2, 2.4)	4.4 (8.4, 6.1)	-6.1 (-11, -9.1)	3.0 (17, 5.8)

TABLE IV

PERFORMANCE METRICS FOR TRACKING REFERENCES OF DIFFERENT FREQUENCIES, WITH RESULTS FORMATTED AS PID+AF (PID, PID+FF).

Period [sec]	MAE [deg]	RMSE [deg]	e_{\max} [deg]	e_{\min} [deg]	Var [deg ²]
10	0.56 (1.6, 0.76)	0.71 (1.9, 1.0)	2.2 (3.9, 2.7)	-2.4 (-5.1, -3.1)	0.50 (3.5, 1.1)
8	0.72 (1.9, 1.0)	0.97 (2.3, 1.5)	2.8 (5.6, 4.1)	-3.1 (-6.6, -5.0)	0.94 (5.4, 2.1)
6	0.86 (2.4, 1.7)	1.3 (3.0, 1.9)	4.5 (6.8, 5.1)	-4.6 (-8.4, -6.4)	1.6 (9.0, 3.6)
4	1.5 (4.6, 1.9)	2.2 (5.4, 2.7)	5.7 (11, 7.4)	-6.5 (-13, -9.4)	4.9 (30, 7.6)
2	3.9 (9.1, 5.4)	5.1 (12, 7.2)	13 (24, 16)	-11 (-22, -17)	26 (130, 51)

REFERENCES

- [1] D. Rus and M. T. Tolley, "Design, fabrication and control of soft robots," *Nature*, vol. 521, no. 7553, pp. 467–475, 2015.
- [2] O. Azami, D. Morisaki, T. Miyazaki, T. Kanno, and K. Kawashima, "Development of the extension type pneumatic soft actuator with built-in displacement sensor," *Sensors and Actuators A: Physical*, vol. 300, p. 111623, 2019. [Online]. Available: <https://www.sciencedirect.com/science/article/pii/S0924424719307538>
- [3] X. Huang, K. Kumar, M. K. Jawed, A. M. Nasab, Z. Ye, W. Shan, and C. Majidi, "Chasing biomimetic locomotion speeds: Creating untethered soft robots with shape memory alloy actuators," *Science Robotics*, vol. 3, no. 25, p. eaau7557, 2018.
- [4] R. Hisatomi, T. Kanno, T. Miyazaki, T. Kawase, and K. Kawashima, "Development of forceps manipulator using pneumatic soft actuator for a bending joint of forceps tip," in *2019 IEEE/SICE International Symposium on System Integration (SII)*, 2019, pp. 695–700.
- [5] T. Miyazaki, T. Tagami, D. Morisaki, R. Miyazaki, T. Kawase, T. Kanno, and K. Kawashima, "A motion control of soft gait assistive suit by gait phase detection using pressure information," *Applied Sciences*, vol. 9, no. 14, 2019. [Online]. Available: <https://www.mdpi.com/2076-3417/9/14/2869>
- [6] H. Lipson, "Challenges and opportunities for design, simulation, and fabrication of soft robots," *Soft Robotics*, vol. 1, no. 1, pp. 21–27, 2014. [Online]. Available: <https://doi.org/10.1089/soro.2013.0007>
- [7] H. Aschemann and D. Schindele, "Comparison of model-based approaches to the compensation of hysteresis in the force characteristic of pneumatic muscles," *IEEE Transactions on Industrial Electronics*, vol. 61, no. 7, pp. 3620–3629, 2013.
- [8] T. Helps and J. Rossiter, "Proprioceptive flexible fluidic actuators using conductive working fluids," *Soft robotics*, vol. 5, no. 2, pp. 175–189, 2018.
- [9] H. Zhao, Y. Li, A. Elsamadisi, and R. Shepherd, "Scalable manufacturing of high force wearable soft actuators," *Extreme Mechanics Letters*, vol. 3, pp. 89–104, 2015.
- [10] C. Laschi and M. Cianchetti, "Soft robotics: new perspectives for robot bodyware and control," *Frontiers in bioengineering and biotechnology*, vol. 2, p. 3, 2014.
- [11] G. Endo and N. Otomo, "Development of a food handling gripper considering an appetizing presentation," in *2016 IEEE International Conference on Robotics and Automation (ICRA)*, 2016, pp. 4901–4906.
- [12] W. M. KIER and K. K. SMITH, "Tongues, tentacles and trunks: The biomechanics of movement in muscular-hydrostats," *Zoological Journal of the Linnean Society*, vol. 83, no. 4, pp. 307–324, 06 2008. [Online]. Available: <https://doi.org/10.1111/j.1096-3642.1985.tb01178.x>
- [13] X. Zang, Y. Liu, S. Heng, Z. Lin, and J. Zhao, "Position control of a single pneumatic artificial muscle with hysteresis compensation based on modified prandtl-ishlinskii model," *Bio-Medical Materials and Engineering*, vol. 28, no. 2, pp. 131–140, 2017.
- [14] F. Schreiber, Y. Sklyarenko, K. Schlüter, J. Schmitt, S. Rost, A. Raatz, and W. Schumacher, "Tracking control with hysteresis compensation for manipulator segments driven by pneumatic artificial muscles," in *2011 IEEE international conference on robotics and biomimetics*. IEEE, 2011, pp. 2750–2755.
- [15] S. Xie, J. Mei, H. Liu, and Y. Wang, "Hysteresis modeling and trajectory tracking control of the pneumatic muscle actuator using modified prandtl-ishlinskii model," *Mechanism and Machine Theory*, vol. 120, pp. 213–224, 2018.
- [16] G. Shi and W. Shen, "Hybrid control of a parallel platform based on pneumatic artificial muscles combining sliding mode controller and adaptive fuzzy cmac," *Control Engineering Practice*, vol. 21, no. 1, pp. 76–86, 2013. [Online]. Available: <https://www.sciencedirect.com/science/article/pii/S0967066112001931>
- [17] X. Zhao and Y. Tan, "Neural network based identification of preisach-type hysteresis in piezoelectric actuator using hysteretic operator," *Sensors and Actuators A: Physical*, vol. 126, no. 2, pp. 306–311, 2006.
- [18] H. Aschemann and D. Schindele, "Comparison of model-based approaches to the compensation of hysteresis in the force characteristic of pneumatic muscles," *IEEE Transactions on Industrial Electronics*, vol. 61, no. 7, pp. 3620–3629, 2014.
- [19] X. Zhu, G. Tao, B. Yao, and J. Cao, "Adaptive robust posture control of a parallel manipulator driven by pneumatic muscles," *Automatica*, vol. 44, no. 9, pp. 2248–2257, 2008. [Online]. Available: <https://www.sciencedirect.com/science/article/pii/S0005109808000654>
- [20] S. Xie, G. Ren, J. Xiong, and Y. Lu, "A trajectory tracking control of a robot actuated with pneumatic artificial muscles based on hysteresis compensation," *IEEE Access*, vol. 8, pp. 80964–80977, 2020.
- [21] C.-P. Chou and B. Hannaford, "Measurement and modeling of mckibben pneumatic artificial muscles," *IEEE Transactions on robotics and automation*, vol. 12, no. 1, pp. 90–102, 1996.
- [22] M.-D. Duong, Q.-T. Pham, T.-C. Vu, N.-T. BUI, and D. Thinh, "Adaptive fuzzy sliding mode control of an actuator powered by two opposing pneumatic artificial muscles," *Scientific Reports*, vol. 13, 05 2023.
- [23] J. Chen, S. Fang, and H. Ishii, "Fundamental limitations and intrinsic limits of feedback: An overview in an information age," *Annual Reviews in Control*, vol. 47, pp. 155–177, 2019.
- [24] H. Li, W. Liu, K. Wang, K. Kawashima, and E. Magid, "A cable-pulley transmission mechanism for surgical robot with backdrivable capability," *Robotics and Computer-Integrated Manufacturing*, vol. 49, pp. 328–334, 2018. [Online]. Available: <https://www.sciencedirect.com/science/article/pii/S0736584516302356>
- [25] K. H. Ang, G. Chong, and Y. Li, "Pid control system analysis, design, and technology," *IEEE transactions on control systems technology*, vol. 13, no. 4, pp. 559–576, 2005.
- [26] A. Visintin, *Differential models of hysteresis*. Springer Science & Business Media, 2013, vol. 111.